JOURNAL OF THEORETICAL AND APPLIED MECHANICS
50, 1, pp. 301-319, Warsaw 2012
50th anniversary of JTAM

ON COMBINED SPATIAL AND TEMPORAL INSTABILITIES OF ELECTRICALLY DRIVEN JETS WITH CONSTANT OR VARIABLE APPLIED FIELD

Saulo Orizaga
Daniel N. Riahi

University of Texas-Pan American, Department of Mathematics, Edinburg, USA
e-mail: driahi@utpa.edu

We investigate the problem of combined spatial and temporal instabilities of electrically driven viscous jets with finite electrical conductivity in the presence of either constant or variable applied electric field. A mathematical model leads to a lengthy equation for the unknown spatial growth rate and temporal growth rate of the disturbances. This equation is solved numerically using Newton's method. We investigated two cases of water jets and glycerol jets. For water jets and in the case of either constant or variable applied field, we found two new modes of instabilities which grow simultaneously in time and space and lead to significant reduction in the jet radius. However, in the case of glycerol jets, we found two new modes of instabilities in the presence of constant applied field but only one mode of instability in the presence of variable applied field. For the glycerol jets, the combined temporal and spatial instabilities are less stronger and lead to an increase in the jet radius. The instabilities for both types of water and glycerol jets were found to be restricted to particular domain in their wavelength and were enhanced with the strength of the electric field.

Key words: temporal instability, spatial instability, jet flow, electric field, jet instability

1. Introduction

In this paper, we consider the problem of combined spatial and temporal instabilities of electrically forced cylindrical jets of a viscous fluid with finite electrical conductivity and in the presence of an externally imposed constant

or variable electric field. The investigations of electrically forced jets are important particularly in applications such as those to electrospraying (Baily, 1988) and electrospinning (Hohman *et al.*, 2001a, 2001b). Electrospinning is a technology that uses electric fields to produce and control small fibers. The aim is at producing non-woven materials that are unparalleled in their porosity, high surface area, and the fineness and uniformity of their fibers. Such a technology has been used in a number of areas including bioengineering, tissue engineering, nano-electronics and in filtration media. Electrospraying is a technology that uses electric field to produce and control sprays of very small drops. The aim is at producing very small drops that are uniform in size and are of charged macromolecules in the gas phase. This technology also has been used in several areas including ink jet printing and the fuel injection process.

There have been a number of theoretical, computational and experimental studies of free shear flows and jets instabilities in the absence of electrical effects (Michalke, 1965; Drazin and Reid, 1981; Tam and Thies, 1993; Soderberg, 2003; Healey, 2008) and in the presence of electrical effects (Taylor, 1969; Reneker *et al.*, 2000; Shkadov and Shutov, 2001; Hohman *et al.*, 2001a, 2001b; Li and Xia, 2004; Yu *et al.*, 2004; Riahi, 2009; Orizaga and Riahi, 2009).

Riahi (2009) followed a modeling approach analog to that due to Hohman *et al.* (2001a) and investigated analytically spatial instability of electrically forced jets with an applied variable field but under a restricted condition of neutral temporal stability and idealistic cases of a jet of zero electrical conductivity or a jet of infinite electrical conductivity and with certain restrictions on the frequency of the disturbances. He detected two spatial modes of instability, each of which was enhanced with increasing the strength of the externally imposed applied electric field. These modes were existed under certain restricted ranges of the axial wave number of disturbances, and, in particular, did not exist if the axial wave number was sufficiently small. Later, Orizaga and Riahi (2009) followed a modeling approach similar to that carried out by Riahi (2009) for the spatial instability of the electrically forced jet and again under a neutral temporal stability condition, but they investigated numerically using Newton's method (Anderson *et al.*, 1984) to determine results based on a set of fluid parameters for the jet with finite conductivity and under a constant or variable applied field. Orizaga and Riahi (2009) found two new modes of spatial instabilities. One of these modes was enhanced by the strength of the applied field, while the other mode decays with increasing the applied field. The growth rates of both modes increased mostly with decreasing the axial wavelength of the disturbances. For the case of a variable applied field, they found the growth rates of the spatial instability modes to be higher than the

corresponding ones for the constant applied field, provided the strength of the applied field was not too small.

In the present study, we first use a method of approach similar to that employed in Riahi (2009) and Orizaga and Riahi (2009) to arrive at a mathematical model for the realistic electrically driven viscous jets with finite conductivity, under externally imposed constant or variable applied field and with no restriction on the neutral stability boundary for the time variation of the superimposed perturbations. Here we consider more realistic jet flow instabilities, where the perturbations grow naturally and simultaneously both in time and space, and so no idealistic marginal stability conditions in time or in space are imposed on the mathematical modeling of the jet flow instability system. We derive the dispersion relation which relates the growth rates of the spatial and temporal instabilities of the growing disturbances to the wave number in the axial direction, the frequency and the non-dimensional parameters of the model. We solve numerically the dispersion relation for the spatial and temporal growth rates of the growing disturbances using Newton's method (Anderson *et al.*, 1984). We found a number of interesting results which were qualitatively different from the earlier studies (Riahi, 2009; Orizaga and Riahi, 2009) where the jet perturbations were not allowed to grow in time. In particular, we found new modes of instability which grow simultaneously in time and space. For the two investigated cases of glycerol and water jets, the growth rates of the modes of instabilities were increased as the strength of the electric field was increased. For the case of water jet, the temporal growth rates were increased mostly, while the spatial growth rates were increased mostly in the case of glycerol jet. The spatial and temporal growth rates for either water jet or glycerol jet decrease mostly with decreasing the axial wave number of the disturbances. For the case of variable applied field, the growth rates of temporal and spatial growing disturbances were found to be mostly higher than the corresponding ones for the case of constant applied field.

2. Formulation and analysis

The present mathematical modeling of the electrically driven jets is based on the governing electrohydrodynamic equations (Melcher and Taylor, 1969), which were already described in some details in Riahi (2009) and Orizaga and Riahi (2009) and, thus, will not be repeated here. Here we briefly describe the physical system and the corresponding mathematical model and refer the reader to these two references for details. A cylindrical, axisymmetric, New-

tonian and incompressible fluid jet is considered to be moving axially with passive air as the external fluid. The governing equations are used in a cylindrical coordinate system with the origin at the center of section where the jet is emitted with the axial z-axis along the axis of the jet. The modeling was based on the approximation that the jet is long and slender in the axial direction with the large length scale in the axial direction in comparison to that in the radial direction, so that a perturbation expansion is used in the small jet aspect ratio. Expanding the dependent variables in the Taylor series in the radial variable r, using such expansions in the full governing axisymmetric system, keeping only the leading terms and non-dimensionalizing the resulting equations, four relatively simple model equations are obtained for the dependent variables h, v, σ and E as functions of t and z. Here h is the radius of the jet cross section, v is the axial velocity, σ is the surface charge, E is the induced electric field and t is the time variable. These equations contain three non-dimensional parameters, which are the conductivity parameter $K^* = K_0\{\rho r_0^3/[\gamma\beta(\widetilde{\varepsilon})^2]\}^{0.5}$, the charge induction parameter $\beta = \varepsilon/\widetilde{\varepsilon} - 1$ and the viscosity parameter $\nu^* = [\nu^2\rho/(\gamma r_0)]^{0.5}$. Here r_0 is radius of the cross-sectional area of the nozzle exit at $z = 0$, γ is the surface tension, K_0 is the reference conductivity, $\varepsilon/(4\pi)$ is the permittivity constant in the jet, $\vartheta\varepsilon/(4\pi)$ is the permittivity constant in the air, ρ is the fluid density and ν is the kinematic viscosity.

Next, the electrostatic equilibrium solution for the four model equations, referred to as the basic state solution, is considered as the one around which perturbations can grow in time and space. The basic state solution for each of the dependent variables, which is designated with a subscript b, is given below

$$\begin{aligned} &h_b = 1 \qquad v_b = 0 \qquad \sigma_b = \sigma_0 \\ &E_b = \frac{\Omega}{\widetilde{K}(z)} = \Omega\Big(1 - \frac{8\sigma_0\pi}{\Omega\sqrt{\beta}}z\Big) \end{aligned} \tag{2.1}$$

where both Ω and σ_0 are constant quantities. Here σ_0 is the background free charge density. We set $\delta = 8\sigma_0\pi/(\Omega\sqrt{\beta})$ to be a small parameter $(\delta \ll 1)$ and consider a series expansion in powers of δ for all the dependent variables for the case of variable applied field.

In this paper, we investigate the cases where the applied electric field can be either constant $(\delta = 0)$ or variable $(\delta \neq 0)$. We consider each dependent variable as sum of its basic state solution plus a small perturbation, which is assumed to be oscillatory in time and in the axial variable. Thus, we write

$$(h, v, \sigma, E) = (h_b, v_b, \sigma_b, E_b) + (h_1, v_1, \sigma_1, E_1) \tag{2.2}$$

where the perturbation quantities, which are designated with subscript 1, are given by

$$(h_1, v_1, \sigma_1, E_1) = (h', v', \sigma', E') \exp[(f + \mathrm{i}\omega)t + (s + \mathrm{i}k)z] \tag{2.3}$$

Here (h', v', σ', E') are small constants, i is the pure imaginary number $\sqrt{-1}$, f is the temporal growth rate of the growing disturbances, ω is the frequency, s is the spatial growth rate of the growing disturbances and k is the axial wave number. Using (2.1)-(2.3) in the four model equations, we linearize with respect to the amplitude of perturbation, consider the lowest order in δ (for the variable applied field case) and divide each equation by the exponential function $\exp[(f+\mathrm{i}\omega)t+(s+\mathrm{i}k)z]$. We then obtain 4 linear algebraic equations for the unknown constants h', v', σ' and E'. To obtain non-trivial (non-zero) values of these constants, the 4×4 determinant of the coefficients of these unknowns must be zero, which yields the following dispersion relation

$$\begin{aligned}
&\frac{1}{2}(k^2 - 1 - s^2 - 2\mathrm{i}ks)(k^2 - s^2 - 2\mathrm{i}ks)\Big[(\mathrm{i}\omega + f)A + \frac{4\pi K^*}{\sqrt{\beta}}\Big] \\
&\quad + (k^2 - s^2 - 2\mathrm{i}ks)\Big[(f + \mathrm{i}\omega)\Big(\frac{12\pi\nu^* K^*}{\sqrt{\beta}} + \frac{\omega^2}{4\pi}\Big) + \frac{\omega^2 K^* A}{\sqrt{\beta}}\Big] \\
&\quad - (\omega - \mathrm{i}f)^2\Big\{\frac{4\pi K^*}{\sqrt{\beta}} + [(f + \mathrm{i}\omega) + 3\nu^*(k^2 - s^2 - 2\mathrm{i}ks)]A\Big\} \\
&\quad + (k - \mathrm{i}s)^2\Big[2(f + \mathrm{i}\omega)A\pi\sigma_0\Big(1 + \frac{\ln 0.89k}{2 + \Lambda}\Big) \\
&\quad + \frac{4\pi K^*}{\sqrt{\beta}}\Big(2\pi\sigma_0^2 - \Omega\sigma_0(s + \mathrm{i}k)\frac{4 + (\ln 0.89k)^{-1}}{(k - \mathrm{i}s)^2\sqrt{\beta}}\Big)\Big] = 0
\end{aligned} \tag{2.4}$$

where

$$A = 1 - \frac{2}{\beta(k - \mathrm{i}s)^2 \ln\frac{1}{\chi}} \qquad \Lambda = -\beta(k - \mathrm{i}s)^2 \ln 0.89k \qquad \chi = \frac{1}{0.89k}$$

It can be seen from lengthy complex equation (2.4) that the spatial growth rate s and temporal growth rate f can be found for given values of the parameters, k and ω. The effects of the unknowns s and f are highly nonlinear in (2.4), and, in particular, it turns out that the solution for s alone with $f = 0$ in (2.4) is quite different from the corresponding solution for s with $f \neq 0$ as our generated data for the two cases verified such outcome.

3. Results and discussion

Dispersion relation (2.4) is investigated for both variable and constant applied field cases. For the variable applied field, where $\delta \neq 0$, we assume that δ is small of order about 0.1, and here both Ω and β cannot take zero value, so that we set $0 < \sigma_0 \leqslant 0.1$, which turns out to keep the maximum value of δ of order 0.1 in the range of values for the rest of the parameters that are considered in the present study. For the constant applied field case, we set $\sigma_0 = 0$. In this Section, we describe each of the cases that we investigated and provide and discuss the corresponding results.

In the present computation, we consider 2 types of fluids for the jet, which can be representatives for those used in the experimental investigation for the problem such as water and a type of glycerol. For such fluids, we set representative values of the parameters to be $K^* = 19.60$, $\nu^*(\text{glycerol}) = = 9.05384$, $\nu^*(\text{water}) = 0.00608$, and $\beta = 77.00$.

In addition, $\sigma_0 = 0$ for the constant applied field and $\sigma_0 = 0.10$ for the variable applied field. We then used (2.4) and carried out Newton's method to generate data for spatial and temporal growth rates, for different values of Ω and for both variable and constant applied field cases. The results are briefly presented in the following two sub-sections.

3.1. The case of water jet

For $\Omega = 1$, we found two new modes of instabilities, each of which grows in both time and space. These modes of instability were present for both cases of constant and variable applied field. The first mode of instability, referred here to as mode I, favors relatively smaller values of the axial wave number k, while the second mode of instability, referred to as mode II, favors relatively larger values of k. For the case of variable applied field, the temporal growth rate for both modes increases with the axial wave number k in the domain $0.04 < k < 0.38$, while the spatial growth rate decreases with increasing k for mode I in $0.36 < k < 0.46$ and increases shapely with k for mode II in $0.70 < k < 0.74$. For the case of constant applied field, the temporal growth rate increases slowly with k for mode I in $0.10 < k < 0.28$) and increases sharply with k for mode II in $0.56 < k < 0.58$, while the spatial growth rate decreases sharply with increasing k for mode I in $0.32 < k < 0.34$ and increases with k for mode II in $0.48 < k < 0.58$.

For $\Omega = 2$, we detected again the presence of two modes I and II of instabilities which grow simultaneously in time and space and operated for

$\Omega = 1$ case described in the previous paragraph. Figures 1 and 2 present results for the growth rates s and f, respectively, versus k for 2 modes I and II and for both constant (dashed lines) and variable (solid lines) applied field cases. As can be seen from Fig. 1, the growth rates s under the constant applied field case decrease with increasing k for mode I in $0.30 < k < 0.38$ and increase with k for mode II in $0.60 < k < 0.64$. For the case of variable applied field, s decreases sharply with increasing k for mode I in $0.36 < k < 0.38$ and increase sharply with k for mode II in $0.58 < k < 0.60$. It can also be seen from Fig. 1 that for the case of variable applied field, the spatial growth rates for mode I are larger than the corresponding ones for the constant applied field case, provided k is in the domain $0.36 < k < 0.38$. The results presented in Fig. 2 for f versus k, indicate that for the variable applied field case, f increases with k in $0.32 < k < 0.38$ for mode I and in $0.50 < k < 0.56$ for mode II. For the constant applied field case, the temporal growth rates increase with k in $0.42 < k < 0.46$ for mode I and in $0.52 < k < 0.56$ for mode II. For the constant applied field case, the temporal growth rates f are greater than the corresponding ones for the variable applied field case, provided the axial wave number is in the domain $0.58 < k < 0.56$.

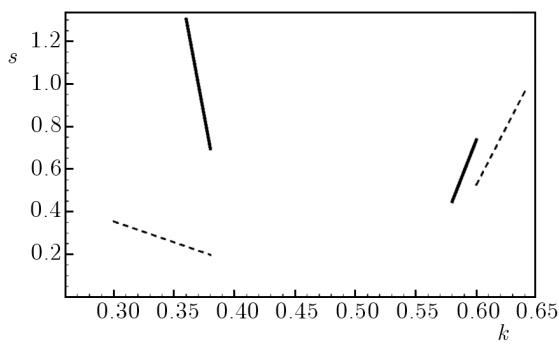

Fig. 1. Spatial growth rate s versus the axial wave number k and for water jet with $\Omega = 2$, constant applied field (dashed lines) and variable applied field (solid lines)

For $\Omega = 3$, the two modes of combined temporal and spatial instabilities continue to operate, where mode I favors relatively smaller values of k and mode II favors relatively larger values of k. For the case of variable applied field, s decreases with increasing k in $0.22 < k < 0.24$ and increases with k in $0.54 < k < 0.58$. Similarly, for the case of constant applied field, s decreases and increases, respectively, with increasing k in $0.28 < k < 0.30$ and $0.60 < k < 0.68$. For the case of constant applied field, s is larger than the corresponding one for the variable applied field case if $0.28 < k < 0.30$. For

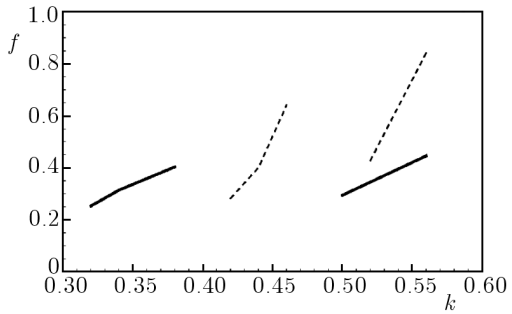

Fig. 2. The same as in Fig. 1 but for the temporal growth rate f versus k

k in $0.54 < k < 0.58$, s is larger for the case of variable applied field. The temporal growth rates under the constant applied field case for both modes increase with k in either $0.30 < k < 0.36$ or $0.76 < k < 0.78$. For the case of variable applied field, f increases with k in either $0.12 < k < 0.24$ or $0.38 < k < 0.46$. For the case of constant applied field, f is larger than the corresponding one for the variable applied field case, provided the axial wave number is in $0.30 < k < 0.36$ or $0.76 < k < 0.78$.

For $\Omega = 4$, we detected again two modes I and II of combined temporal and spatial instabilities which favor relatively smaller and larger values of k, respectively. We generated data for either constant $(\sigma_0 = 0)$ or variable $(\sigma_0 \neq 0)$ applied field case. The growth rates s increase with k depending on the range of value for the axial wave number. For $\sigma_0 = 0$, s decreases and increases with increasing k for k in $0.38 < k < 0.40$ and $0.60 < k < 0.62$, respectively. For $\sigma_0 = 0.1$, we found that s decreases and increases with increasing k for k in $0.26 < k < 0.30$ and $0.68 < k < 0.72$, respectively. For the case of constant applied field, the spatial growth rates are larger than the corresponding ones for the variable applied field if k lies in the domain $0.38 < k < 0.40$. The temporal growth rate was found to increase with k for both modes I and II and under either constant or variable applied field case.

Figures 3 and 4 present s and f versus k, respectively, for the case of constant applied field but different values of Ω. We can see from Fig. 3 that larger values of the strength of the applied field can lead to higher values of the spatial growth rate for particular values of the wave numbers for both modes I and II. It can be seen from Fig. 4 that for mode I, the temporal growth rate increases with increasing Ω for k in the domain $0.16 < k < 0.26$, while f can have higher value for larger value of Ω in the domain $0.68 < k < 0.70$ for k.

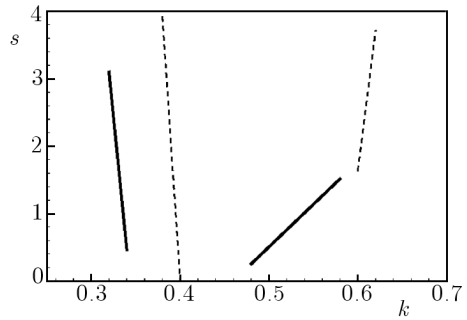

Fig. 3. Spatial growth rate s versus the axial wave number k for constant applied field and for water jet with two values of $\Omega = 1$ (solid line) and 4 (dashed line)

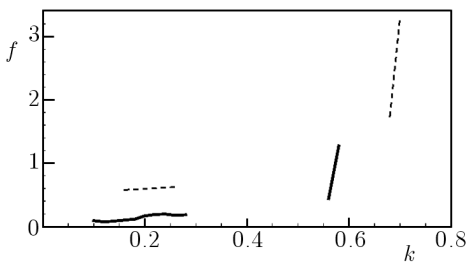

Fig. 4. The same as in Fig. 3 but for the temporal growth rate f versus k

Figures 5 and 6 present s and f versus k, respectively, for the case of variable applied field and different values of Ω. It can be seen from both these figures that the spatial or temporal growth rates for both modes I and II can have higher values for larger values of Ω.

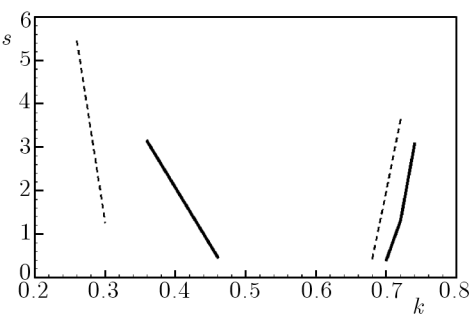

Fig. 5. Spatial growth rate s versus the axial wave number k for variable applied field and for water jet with two values of $\Omega = 1$ (solid line), and 4 (dashed line)

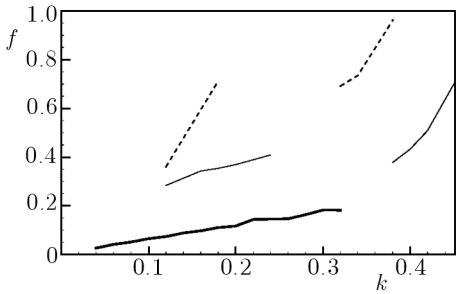

Fig. 6. Temporal growth rate f versus the axial wave number k for variable applied field and for water jet with three values of $\Omega = 1$ (thick-solid line), 3 (thin-solid line) and 4 (dashed line)

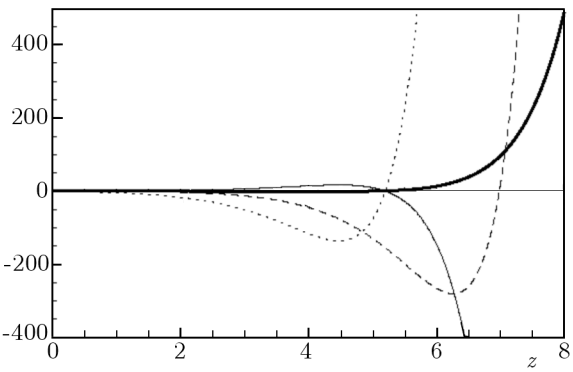

Fig. 7. Perturbation quantities h_1 (thin solid line), v_1 (dashed line), σ_1 (thick solid line) and E_1 (dotted line) versus the axial variable z for water jet with $\Omega = 4$, $\sigma_0 = 0.1$, $t = 1$, $k = 0.38$, $s = 1.346087$ and $f = 0.961981$

Figure 7 presents variations of the perturbation quantities for mode I of combined spatial and temporal instabilities versus the axial variable z and for $\sigma_0 = 0.1$, $\Omega = 4$, $k = 0.38$, $s = 1.3460$ and $f = 0.9619$ but at one given instant in time $(t = 1)$. Due to the linear instability of the problem, we set $h' = 0.1$ and determined the other perturbation constants v', σ' and E' using the procedure described in the previous Section. The real parts of the perturbation quantities are used to collect the perturbation data for the instability mode for different values of z. It can be seen from this figure that most of the perturbation quantities begin to grow spatially after their generation at $z = 0$ and their spatial growth is seen mainly as an exponential type of growth for values of z beyond $z = 6$ or so. For $z > 6.4$, the amplitudes of the perturbations for v_1 and h_1 are sufficiently large that the present linear theory ceases to be valid. In addition and most importantly, it is seen that the jet radius

perturbation can become negative for $z > 5.6$ and the magnitude increases rapidly with increasing z. Using this result together with $(2.1)_1$ and (2.2), it implies significant reduction in the jet radius by the instabilities of mode I. This result can have important implication with respect to the electrospinning applications and making use of instabilities in a controlling manner for production of very small- and nano-scale fibers. Figure 8 presents variations of the perturbation quantities for mode I of combined spatial and temporal instabilities versus time variable t for $\sigma_0 = 0.1$, $s = 1.3460$, $k = 0.38$, $f = 0.9619$ and $\Omega = 4$ but at one given axial location $(z = 1)$. Again it can be seen that, for example, for $t > 5.4$, the amplitude of v_1 and E_1 are sufficiently large that the linear theory ceases to be valid. In addition, temporal instability of mode I also exhibits significant reduction in the jet radius, which is enhanced with increasing time. From the results presented in the Figs. 7 and 8, which were for the case of variable applied field, it can be concluded that combined spatial and temporal instabilities exhibit both significant reduction in the jet radius and a higher sensitivity of the jet flow with respect to the disturbances that can grow simultaneously in time and in space. We also generated similar data for the case of constant applied field and found that the spatial and temporal instabilities are more effective and enhanced in the case of variable applied field.

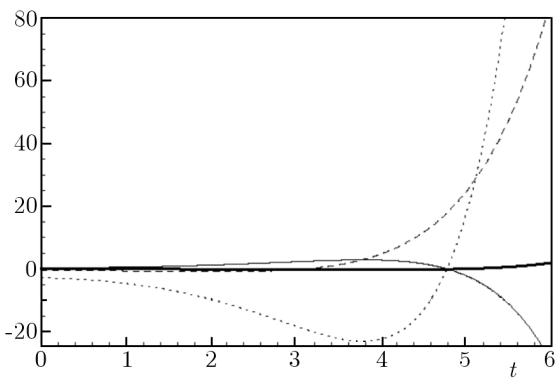

Fig. 8. Perturbation quantities h_1 (thin solid line), v_1 (dashed line), σ_1 (thick solid line) and E_1 (dotted line) versus the axial variable t for water jet with $\Omega = 4$, $\sigma_0 = 0.1$, $z = 1$, $k = 0.38$, $s = 1.3460$ and $f = 0.9619$

3.2. The case of glycerol jet

For $\Omega = 1$, we found two modes of combined temporal and spatial instabilities similar to modes I and II described earlier in the case of water (sub-section 3.1) that were present for the case of constant applied field. For

this case, the growth rates s increase with the axial wave number in either $0.14 < k < 0.26$ or $0.92 < k < 0.96$, while the growth rates f remain quite small and non-monotonic for k in either $0.24 < k < 0.48$ or $0.50 < k < 0.70$. For the case of variable applied field, only one mode of combined temporal and spatial instability was detected, which favored relatively intermediate or large values of k. For this case, s increases with k in $0.84 < k < 0.98$, while f decreases with increasing k in $0.30 < k < 0.38$.

For $\Omega = 2$, we found the two modes of instabilities continue to be present under the case of constant applied field. For this case, s increases with k in either $0.02 < k < 0.16$ or $0.58 < k < 0.98$, while f increases with k in either $0.06 < k < 0.16$ or $0.22 < k < 0.28$. For the case of variable applied field, we found that s decreases with increasing the axial wave number in $0.16 < k < 0.32$ and increases with k in $0.38 < k < 0.98$, while the temporal growth rate decreases with increasing k in $0.04 < k < 0.28$. For the case variable applied field, the spatial growth rates are larger than the corresponding ones for the constant applied field case, provided k is in the domain $0.66 < k < 0.98$. For the case of constant applied field, the temporal growth rates are larger than those for the variable applied field case, provided the axial wave number lies in $0.22 < k < 0.26$.

Figures 9 and 10 present the growth rates s and f, respectively, versus the wave number k for both cases of constant and variable applied field. It can be seen from Figs. 9 and 10 that the spatial growth rates are enhanced by the presence of variable applied field, while the temporal growth rates are enhanced by the variable field only if the axial wave number is sufficiently small.

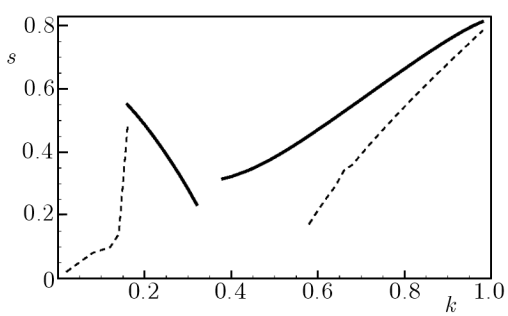

Fig. 9. Spatial growth rate s versus the axial wave number k for glycerol jet with $\Omega = 2$, constant applied field (dashed lines) and variable applied field (solid lines)

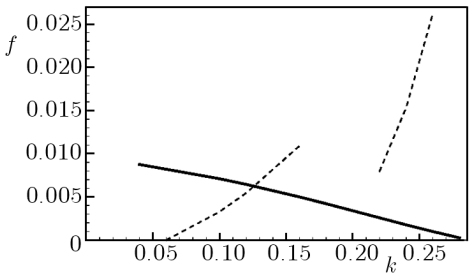

Fig. 10. The same as in Fig. 9 but for the temporal growth rate f versus k

For $\Omega = 3$, again there are two modes of combined temporal and spatial instabilities under the constant applied field case. In this case, s increases with k in either $0.16 < k < 0.44$ or $0.50 < k < 0.98$. For the case of variable applied field, s increases with k in $0.16 < k < 0.98$. For the case of variable applied field, s is larger than the corresponding one for the constant applied field case if k lies in $0.16 < k < 0.44$. The growth rates of temporal instabilities under either constant or variable applied field were found to remain very close to zero of order about $10\exp(-17)$ or smaller for all the values of k in the domain $0 < k < 1$.

For $\Omega = 4$, we found that the two modes of combined temporal and spatial instabilities continue to exist for the case of constant applied field. The growth rates s increase with k in either $0.24 < k < 0.44$ or $0.52 < k < 0.98$, while the growth rates f increase and decrease, respectively with increasing k in $0.04 < k < 0.12$ and $0.48 < k < 0.70$. For the case of variable applied field, we found that s increases with k in the domain $0.26 < k < 0.98$, but f decreases with increasing k in the domain $0.16 < k < 0.30$. For the case of variable applied field, the spatial growth rates are larger than the corresponding ones for the temporal growth rates if k lies in $0.24 < k < 0.44$. For the case of constant applied field, the temporal growth rates were found to be larger than the corresponding ones for the variable applied field if k is in the domain $0.06 < k < 0.12$. Figures 11 and 12 present the growth rates s and f, respectively, versus k for the case of constant applied field and for different values of Ω. It can be seen from these figures that the spatial or temporal growth rates can be enhanced by the strength of the applied field. For f, we found increasing and decreasing modes of instability along the axial wave number. Figures 13 and 14 present s and f, respectively, versus k for the case of variable applied field and for different values of Ω. As can be seen from these figures, the spatial growth rates can be enhanced by the strength of the applied field, while the temporal growth rates can be decreased by increasing the strength of the field.

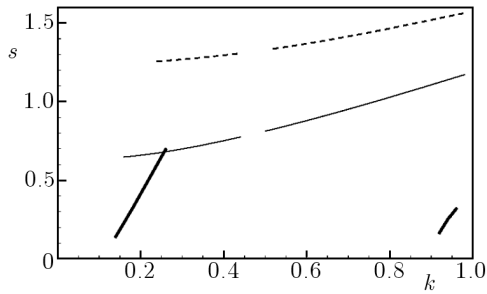

Fig. 11. Spatial growth rate s versus the axial wave number k for glycerol jet with constant applied field and for three values of $\Omega = 1$ (solid line), 3 (thin line) and 4 (dashed line)

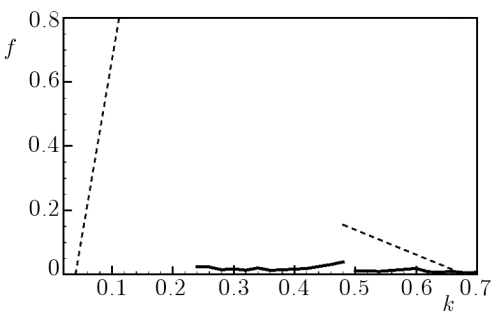

Fig. 12. Temporal growth rate f versus the axial wave number k for glycerol jet with constant applied field and for two values of $\Omega = 1$ (thick line) and 4 (dashed line)

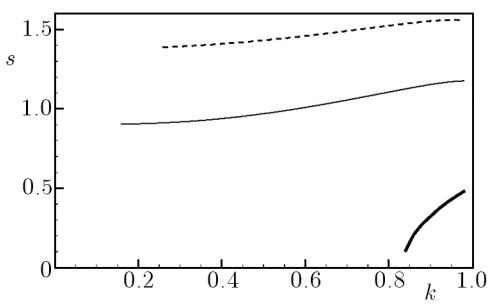

Fig. 13. Spatial growth rate s versus the axial wave number k for glycerol jet with variable applied field and for three values of $\Omega = 1$ (solid line), 3 (thin line) and 4 (dashed line)

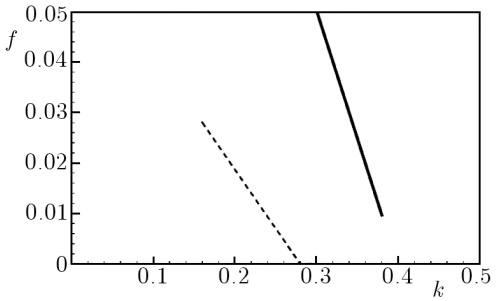

Fig. 14. Temporal growth rate f versus the axial wave number k for glycerol jet with variable applied field and for two values of $\Omega = 1$ (thick line) and 4 (dashed line)

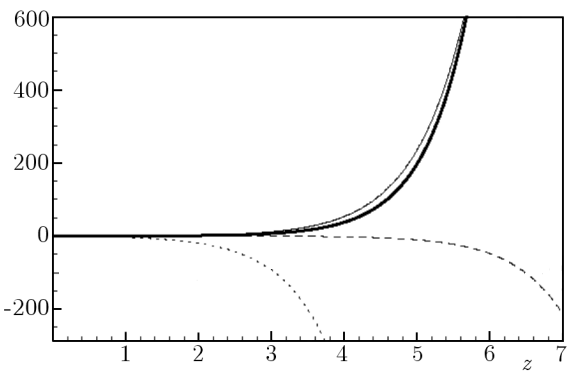

Fig. 15. Perturbation quantities h_1 (thin solid line), v_1 (dashed line), σ_1 (thick solid line) and E_1 (dotted line) versus the axial variable z for glycerol jet with $\Omega = 4$, $\sigma_0 = 0.1$, $t = 1$, $k = 0.16$, $s = 1.6251$ and $f = 0.0280$

Figure 15 presents variations of the perturbation quantities versus the axial variable z for $\sigma_0 = 0.1$, $\Omega = 4$, $k = 0.16$, $s = 1.6251$ and $f = 0.0280$ but at one given instant in time $(t = 1)$. It can be seen from this figure that most of the perturbation quantities begin to grow spatially after their generation at $z = 0$ and their spatial growth is seen mainly as an exponential type of growth for values of z beyond $z = 4.5$ or so. For $z > 5.5$, the amplitudes of perturbations for σ_1 and h_1 are sufficiently large that the present linear theory ceases to be valid. In addition, it can be seen that in contrast to the case of water jet, the glycerol jet radius is enhanced by the mode of instability. Figure 16 presents variations of the perturbations versus time t for $\Omega = 4$, $k = 0.16$, $\sigma_0 = 0.1$, $s = 1.6251$ and $f = 0.0280$ but for a given location in the axial direction $(z = 1)$. Again it can be seen that, for example, for $t > 55$, the

amplitude of E_1 is sufficiently large that the linear theory ceases to be valid. It is also seen that the jet radius is increased with time. Comparing the results presented in Figs. 7, 8, 15 and 16, it can be concluded that in the presence of variable applied field, combined spatial and temporal instabilities exhibit higher strength and sensitivity and can lead to significant reduction in the jet radius, while such instabilities exhibit lower strength and sensitivity and lead to an increase in the jet radius in the case of glycerol jets. Our additional collected data for the constant applied field and for both water and glycerol jets lead to similar conclusions stated above.

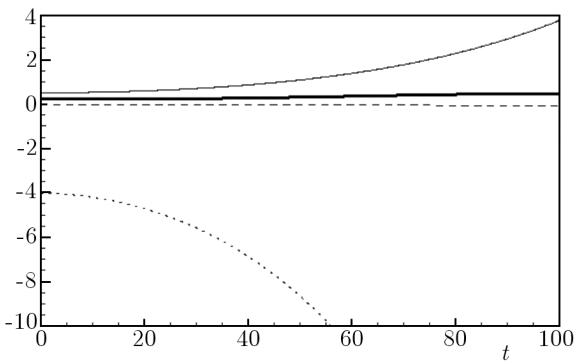

Fig. 16. Perturbation quantities h_1 (thin solid line), v_1 (dashed line), σ_1 (thick solid line) and E_1 (dotted line) versus the axial variable t for glycerol jet with $\Omega = 4$, $\sigma_0 = 0.1$, $z = 1$, $k = 0.16$, $s = 1.6251$ and $f = 0.0280$

4. Concluding remarks

Mathematical modeling and numerical investigation of combined linear spatial and temporal instabilities of electro-hydrodynamic system for electrically forced slender viscous and finite conducting jet flows with externally imposed either constant or variable applied field were carried out. We were able to uncover two new modes of instabilities in the case of water jet in presence of either constant or variable applied field. For the case of glycerol jet, we found two modes of combined temporal and spatial instabilities under the imposed constant applied field and only one such a mode in the case of variable applied field. For the case of variable applied field, only one mode of instability was found for the glycerol jet. The detected temporal-spatial instabilities were found to reduce significantly the jet radius and exhibit higher strength and

sensitivity in the water jet cases, in which the jet radius is enhanced and instabilities are less strong with lower sensitivity in the case of glycerol jets. In addition, it was found that the instability modes are more effective mostly in the case of variable applied field.

In regard to the relevance of the present detected modes of combined temporal and spatial to the available experimental results (Taylor, 1969; Hohman *et al.*, 2001a,b) and in applications, we note that for electrically forced jets, Taylor (1969) documented the presence of axisymmetric instabilities at lower values of the strength of the applied field and non-axisymmentric whipping modes of instabilities at higher values of the field strength. Hohman *et al.* (2001a,b) observed experimentally axisymmetric excitations and growth in time as well as thickening blobs along the axial direction, and instabilities appeared to grow in time as well as they move downstream. These observations indicate the presence of axisymmetric instabilities and also temporally and spatially growing disturbances in the jet flow. Since non-axisymmetric whipping modes of instabilities have also been observed to be strong leading to significant jet radius reduction and ultimately break up the jets (Hohman *et al.*, 2001b), it was thought that the whipping mode is the important instability mechanism for jet radius reduction and the corresponding advantage for controlling such instability in order to produce higher quality fibers of very small- and nano-scale size. However, the present results for the axisymmetric modes of combined temporal and spatial instabilities in water jets, that can lead to significant reduction in the jet radius, could stimulate future investigations for ways to make use of such results in an optimized manner to production of higher quality fiber materials.

Further extensions of the present study that are planned by the second author to be investigated in future, are the cases of combined spatial and temporal instabilities due to the non-axisymmetric disturbances. As is evident from the well known experiments by Taylor (1969) that the electrically forced jets can be non-axisymmetric and whip for sufficiently large values of the strength of the electric field, we can expect that combined spatial and temporal instabilities due to the non-axisymmetric disturbances can dominate over the corresponding axisymmetric ones if Ω is sufficiently large.

Acknowledgement

This research was supported by a research grant from UTPA-FRC.

References

1. Anderson D.A., Tannehill R.H., Pletcher R.H., 1984, *Computational Fluid Mechanics and Heat Transfer*, Hemisphere Publishing Corporation, New York
2. Baily A.G., 1988, *Electro-Static Spraying of Liquid*, Wiley, New York
3. Drazin P.G., Reid W.H., 1981, *Hydrodynamic Stability*, Cambridge University Press, UK
4. Healey J.J., 2008, Inviscid axisymmetric absolute instability of swirling jets, *Journal of Fluid Mechanics*, **613**, 1-33
5. Hohman M. M., Shin M., Rutledge G., Brenner M.P., 2001a, Electrospinning and electrically forced jets. I. Stability theory, *Phys. of Fluids*, **13**, 8, 2201-2220
6. Hohman M.M., Shin M., Rutledge G., Brenner M.P., 2001b, Electrospinning and electrically forced jets. II. Applications, *Phys. of Fluids*, **13**, 8, 2221-2236
7. Li D., Xia Y., 2004, Direct fabrication of composite and ceramic hollow nanofibers by electrospinning, *Nano Letters*, **4**, 933-938
8. Melcher J.R., Taylor G.I., 1969, Electrohydrodynamics: A review of the interfacial shear stresses, *Annual Review of Fluid Mechanics*, **1**, 111-146
9. Michalke A., 1965, On spatially growing disturbances in an inviscid shear layer, *Journal of Fluid Mechanics*, **23**, 521-544
10. Orizaga S., Riahi D.N., 2009, Spatial instability of electrically driven jets with finite conductivity and under constant or variable applied field, *Applications and Applied Mathematics: An International Journal*, **4**, 2, 249-262
11. Reneker D.H., Yarin A.L., Fong H., 2000, Bending instability of electrically charged liquid jets of polymer solutions in electrospinning, *Journal of Applied Physics*, **87**, 4531-4547
12. Riahi D.N., 2009, On spatial instability of electrically forced axisymmetric jets with variable applied field, *Applied Mathematical Modeling*, **33**, 3546-3552
13. Shkadov V.Y., Shutov A.A., 2001, Disintegration of a charged viscous jet in a high electric field, *Fluid Dynamic Research*, **28**, 23-29
14. Soderberg D.L., 2003, Absolute and convective instability of a relaxational plane liquid jet, *Journal of Fluid Mechanics*, **439**, 89-119
15. Tam C.K.W., Thies A.T., 1993, Instability of rectangular jet, *Journal of Fluid Mechanics*, **248**, 425-448
16. Taylor G.I., 1969, Electrically driven jets, *Proceedings of the Royal Society of London, Series A*, **313**, 453-475

17. Yu J.H., Fridrikh S.V., Rutledge G.C., 2004, Production of submicrometer diameter fibers by two-fluid electrospinning, *Advanced Materials*, **16**, 1562-1566

O złożonych, przestrzenno-czasowych niestabilnościach elektrycznie indukowanych strumieni w stałym i zmiennym polu

Streszczenie

Autorzy prezentują problem złożonych przestrzenno-czasowych niestabilności elektrycznie indukowanych strumieni wiskotycznych o skończonej przewodności elektrycznej w obecności stałego albo zmiennego pola. Model matematyczny sprowadzono do skomplikowanego równania, w którym niewiadomą jest czasowe i przestrzenne tempo wzrostu zakłóceń w strumieniu. Równanie to rozwiązano numerycznie, używając metody Newtona. Zbadano dwa przypadki – dla strumienia wody i gliceryny. Dla wody, niezależnie od tego, czy pole elektryczne jest stałe, czy zmienne, wykryto dwie nowe postacie niestabilności rosnących równocześnie w czasie i przestrzeni, które znacznie ograniczają promień strumienia. W przypadku gliceryny, dwie nowe postacie niestabilności znaleziono tylko przy stałym polu elektrycznym. W polu zmiennym zaobserwowano jedną postać. Dla gliceryny, złożone niestabilności przestrzenno-czasowe wykazują słabszą intensywność i zwiększają promień strumienia. Niezależnie od rodzaju ośrodka, niestabilności te ograniczają się do pewnego zakresu długości falowej i wzrastają z natężeniem pola elektrycznego.

Manuscript received August 9, 2010; accepted for print June 20, 2011